JOC The Journal of Organic Chemistry

ARTICLE

pubs.acs.org/joc

Asymmetric Imine *N*-Inversion in 3-Methyl-4-pyrimidinimine. Molecular Dipole Analysis of Solvation Effects

Stephanie Coyle and Rainer Glaser*

Department of Chemistry, University of Missouri, Columbia, Missouri 65211, United States

Supporting Information

ABSTRACT: The thermal (*E*)/(*Z*)-isomerization of 3-methyl-4-pyrimidinimine, 3MePMI, has been studied in the gas phase at MP2/6-31G* and with the inclusion of medium effects using the polarizable continuum method, PCM(MP2/6-31G*), and the solvation model density method, SMD(MP2/6-31G*). For the free molecule and for 3MePMI in each of 14 solvents, the structures were determined of the (*E*)- and (*Z*)-isomers, of the transition state structure for isomerization ITS by asymmetric *N*-inversion, and of the second-order saddle point structure (SOSP) associated with in-plane *N*-inversion. The results predict a reduction of the (*E*)-isomer preference energy of 3MePMI, an increase of the deformation energy $\Delta E_{def} = E(\text{SOSP}) - E(\text{ITS})$, and an increase of the activation barrier $E_{act}(Z \rightarrow E)$ with increasing solvent polarity. Electronic effects associated with *N*-inversion are analyzed using molecular orbital theory, results of population analysis, and electrostatic potential maps. The molecular dipole moments are superior parameters for the description of electronic relaxation in the imine basin during *N*-inversion. In particular, the analysis of dipole moments explains the compatibility of the increase of local CN polarity during *N*-inversion with the negative solvation effect on the activation barrier.

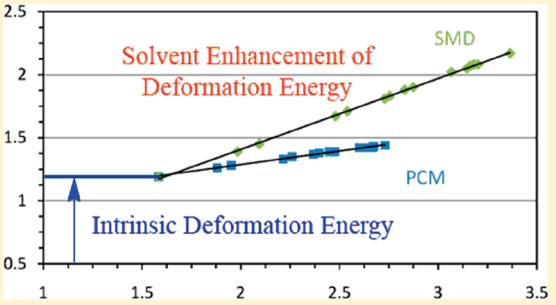

INTRODUCTION

The (*E*)/(*Z*)-isomerization of imines can occur via acid catalysis,[1] base catalysis,[2,3] or without catalysis, and we are interested in the thermal uncatalyzed isomerization of imines via *N*-inversion. The barriers of (*E*)/(*Z*)-isomerization have been characterized for a variety of nonexocyclic imines. *N*-Alkyl benzophenone imines (ArAr′C═N−R) in cyclohexane were measured to have ΔE_a around 25 kcal/mol depending on the temperature.[4a] In later studies, the activation energies of *N*-alkyl and *N*-aryl benzophenone imines in a variety of solvents were characterized by Curtin et al.[4b] (in cyclohexane, heptane, and ethanol) and by Jennings et al.[5] (in diethyl ether, toluene, and *tert*-butyl alcohol). Depending on the arene substituent, the activation energies of these *N*-alkyl and *N*-aryl imines were between 17 and 30 kcal/mol. Imines of the type R−CPh═N−Ph were estimated to have a rate constant of 27 s^{-1} (ca. 50 °C) and a $\Delta G^{\ddagger}$ of 16.8 kcal/mol[6] for the (*E*)/(*Z*) isomerization. Various formimines H_2C═N−X (X = CN, H, $^{+}$N≡N:, OH, F) were computed with the 6-31G basis set and were found to proceed via in-plane *N*-inversion transition state structures and with a wide variety of inversion barriers from 14 to 78 kcal/mol depending on X.[7] Gálvez and Guirado recently reported a more extensive study of aliphatic imines R_2C═N−X (X = H, OR, NH_2, CH_3, $COOCH_3$, CN, NO_2, Cl, Ph) and also found barriers of 10−70 kcal/mol.[8] Interestingly, this study showed that C═N isomerization might involve *N*-inversion, rotation, or intermediate cases depending on the nature of R.

We have been interested in the *N*-inversion of pyrimidine-4(3*H*)-imine, PMI, a precursor to 4-aminopyrimidine, APM (Scheme 1). Computations by Öğretir and Yaman showed a preference for APM over PMI of 14−15 kcal/mol[9] depending on the AM1, PM3, or MNDO method used. Smets et al. computed a slightly higher preference of about 21.5 kcal/mol at the RHF/6-31++G(d,p) level for APM over (*Z*)-PMI.[10] Recently, we studied the relative stability of the (*E*)/(*Z*)-isomers of PMI and the mechanism of their *N*-inversion in detail. The (*E*)-isomer is the most stable isomer with a preference ΔE = 3.1 kcal/mol over the (*Z*)-isomer and an activation barrier $E_A(Z \rightarrow E)$ of 24.3 kcal/mol at the MP2 level.[11] We found that nonplanar *N*-inversion transition state (ITS) structures occur along enantiomeric reaction paths and stationary structures for in-plane *N*-inversion correspond to second-order saddle points (SOSP) on the potential energy surface. The nonplanar ITS structure is preferred over its adjacent SOSP structure by a deformation energy $\Delta E_{def} = E(\text{SOSP}) - E(\text{ITS})$ which is less than 0.9 kcal/mol.[11] The discussion of the asymmetry along the *N*-inversion processes in the heteroarene imines points out the possibility for the occurrence of enantiomeric *N*-inversion paths, and the modest magnitude of the energy difference ΔE_{def} makes the study of solvent effects on the *N*-inversion imperative. One must ask whether the chiral isomerization paths are real and whether it

Received: February 26, 2011
Published: April 28, 2011

Scheme 1. (*Z*)/(*E*)-Isomerization of Pyrimidine-4(3*H*)-imine and 3-Methyl Pyrimidine-4(3*H*)-imine in Context

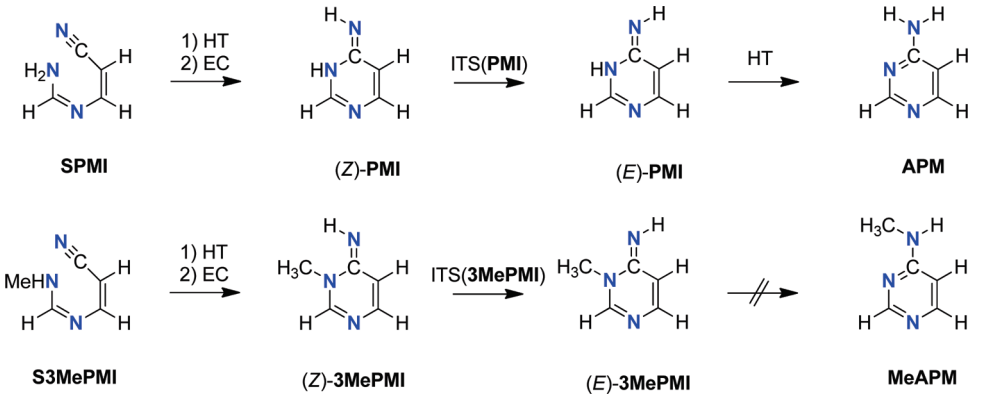

Scheme 2. Options for C═N Isomerization and Imine N-Hybridization

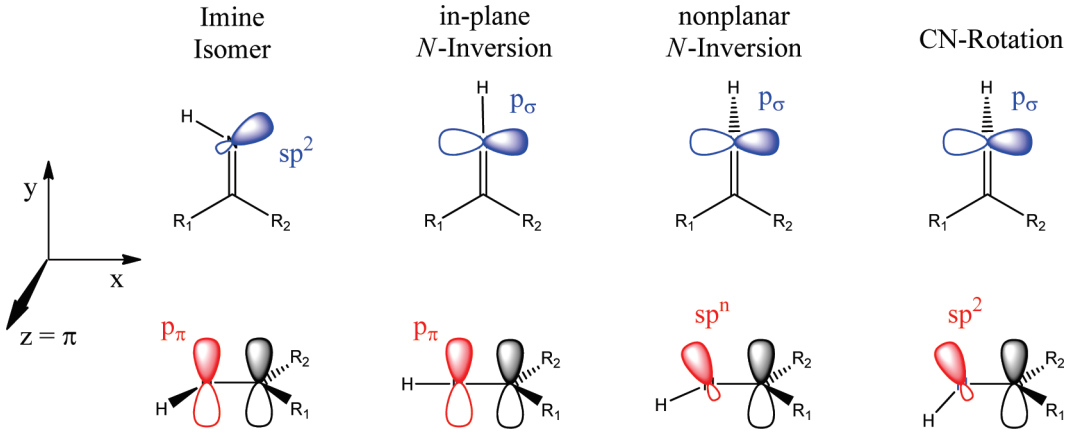

is possible to use to solvent to affect the isomer preference and the deformation energy.

The direct experimental observation of *N*-inversion in PMI is not possible because PMI readily undergoes hydrogen transfer of the H at N3 to yield APM. On the other hand, 3-methyl-4-pyrimidinimine, 3MePMI, cannot react further to form *N*-methyl-4-aminopyrimidine, MeAPM, and hence 3MePMI is the ideal candidate for study. We report here the results of an ab initio study of the effects of solvent polarity on the *N*-inversion path of 3MePMI. The structures of the isomeric minima, of the transition state structure for isomerization, and of the associated second-order saddle point structure of 3MePMI were determined for 14 solvents that cover the range of organic solvent polarity (heptane, benzene, diethyl ether, chloroform, aniline, THF, methylene chloride, dichloroethane, acetone, ethanol, methanol, acetonitrile, DMSO, and water). Solvation effects are discussed on structures and relative isomer preference energies IPE, on deformation energies E_{def}, and on activation barriers $E_A(Z \rightarrow E)$ as a function of solvent polarity. The solvent effects on the molecular dipole moments are superior indicators of changes to the electron density distribution in the imine-N basins[12] because the dipole moments of lone pairs are large in magnitude[13−17] and because *N*-inversion is associated with major changes of their orientations. We computed the molecular dipole moments relative to the molecular dipole moment of the respective in-plane *N*-inversion structure, identified the relative dipole moments with the imine-N lone pair dipole moments, and examined solvation effects on the N-lone pair dipole moments and their relations to energy parameters of the *N*-inversion reaction.

COMPUTATIONAL METHODS

Potential energy surface (PES) analysis[18] using second-order Møller−Plesset perturbation theory (MP2)[19,20] was employed in conjunction with the 6-31G* basis set,[21] MP2(full)/6-31G*, to locate and characterize the (*E*)- and (*Z*)-minima, the transition state structures, and the second-order saddle points structures. The structures were determined for the free molecules and with the inclusion of effects of solvation.

Solvation can be modeled by continuous and discrete solvent models,[22] and we employed two methods of density-based, self-consistent reaction field theory of bulk electrostatics (SCRF). In the polarizable continuum method[23,24] (PCM), the solvent is treated as a continuous polarizable medium characterized but its dielectric constant (ε) and the solute's cavity is defined by overlapping spheres with radii r_k of the solute's atoms *k*. The solute's energy in solution is determined by making the solvent reaction field self-consistent with the solute's electrostatic potential. In addition, we employed the recently developed solvation model density (SMD) method.[25,26] The SMD method accounts for long-range electrostatic polarization (bulk solvent) and also for short-range effects associated with cavitation, dispersion, and solvent structural effects (CDS). The computation of the bulk effects parallels the PCM approach; it requires the dielectric constant of the solvent and

dx.doi.org/10.1021/jo200411f |*J. Org. Chem.* 2011, 76, 3987–3996

Table 1. Relative Isomer Stabilities and Activation Energies Computed for the Gas-Phase Reaction and the Reaction in Chloroform and Aqueous Solution

medium, dielect const	parameter[a]	ΔE_r (Z) vs (E)	ΔE_A (E) → ITS	ΔE_A (Z) → ITS	ΔE_{def} SOSP vs ITS
gas phase, 1.0			MP2(full)/6-31G*		
	ΔE	3.96	27.29	23.33	1.19
	ΔH_0	3.83	25.41	21.58	0.67
	ΔH_{298}	3.83	25.51	21.68	0.56
	ΔG_{298}	3.82	25.33	21.51	0.70
chloroform, 4.90			PCM(MP2(full)/6-31G*)		
	ΔE	3.17	27.32	24.15	1.35
	ΔH_0	3.19	25.26	22.07	0.78
	ΔH_{298}	3.19	25.37	22.18	0.68
	ΔG_{298}	3.19	25.16	21.97	0.77
			SMD(MP2(full)/6-31G*)		
	ΔE	2.44	27.49	25.04	1.71
	ΔH_0	2.48	25.51	23.03	1.23
	ΔH_{298}	2.43	25.56	23.14	1.13
	ΔG_{298}	2.58	25.50	22.92	1.25
water, 78.39			PCM(MP2(full)/6-31G*)		
	ΔE	3.01	27.45	24.44	1.44
	ΔH_0	3.09	25.33	22.25	0.84
	ΔH_{298}	3.08	25.44	22.36	0.74
	ΔG_{298}	3.09	25.23	22.15	0.84
			SMD(MP2(full)/6-31G*)		
	ΔE	1.76	27.74	25.98	2.17
	ΔH_0	1.67	25.54	23.87	1.40
	ΔH_{298}	1.67	25.66	23.98	1.40
	ΔG_{298}	1.63	25.40	23.78	1.22

[a] All data in kcal/mol.

the determination of the solvent accessible surface (SAS) based on atom-centered spheres with intrinsic Coulomb radii F_k. The computation of the short-range CDS term requires parameters for the atomic surface tensions (σ_k) of atoms k, for the molecular surface tension $\sigma^{[M]}$, and for the solvent accessible surface area A_k of atoms k. The atomic and molecular surface tensions depend on three solvent properties: the solvent's refractive index n, Abraham's hydrogen bond acidity parameter α, and Abraham's hydrogen bond basicity parameter β. The A_k values are computed with the knowledge of the solute atoms' van der Waal radii and the solvent radius (r_S). The SMD parametrization is based on an extensive set of 2821 solvation data including neutral and charged solutes in aqueous and nonaqueous solvents.[25] Below, we graph the computed solvation effects as a function of solvent dielectric constant, and the resulting line plots are generally fairly smooth. Noticeable deviations occur for the protic solvents (ROH, H_2O) in the SMD computations because of the CDS terms.

For each solvent, the four stationary structures were optimized at the PCM(MP2(full)/6-31G*) and SDM(MP2(full)/6-31G*) levels using *Gaussian09*[27] in conjunction with *Gaussview 5*,[28] and these levels are referred to as PCM and SMD for brevity. Total energies (E_{tot}), vibrational zero point energies (VZPE), thermal energies (TE), molecular entropies (S), the numbers of imaginary frequencies (NI), and the lowest vibrational frequencies ν_1 and ν_2 computed at the PCM and SMD levels, respectively, are given in Tables S1 and S2 of the Supporting Information together with respective data computed for the gas-phase reaction. In Table 1 are listed the relative energies computed for the gas phase reaction and for aqueous solution at the PCM and SMD levels, respectively. The columns of Table 1 list the values of the isomer preference energy $\Delta E_r = \Delta E(Z \text{ vs } E)$, the activation energies $\Delta E_A(E \rightarrow \text{ITS})$ and $\Delta E_A(Z \rightarrow \text{ITS})$, and the deformation energy $\Delta E_{def} = \Delta E(\text{SOSP vs ITS})$ determined for each solvent. For each of these parameters, four thermodynamic values are provided: ΔE, ΔH_0, ΔH_{298}, and ΔG_{298}. Table S3 contains the respective data for all solvents studied.

RESULTS AND DISCUSSION

Imine Isomerization Type and *N*-Hybridization. The in-plane *N*-inversion process retains one N_σ-lone pair, and this lone pair changes shape from approximately sp^2 in the imine to p_σ in the inversion transition state structure. In-plane *N*-inversion leaves the direction of the p_π-AO at the imine-N unchanged, while nonplanar *N*-inversion allows for *N*-rehybridization from p_π to sp^n. The nature of *N*-rehybridization in the transition state structure is key and allows for the characterization of options for C═N isomerization (Scheme 2).

The imine N_σ-lone pair contains contribution from the s-, p_x- and p_y-AOs at nitrogen. The in-plane *N*-inversion transition state structure contains only p_x-AO in its p_σ lone pair; the s- and p_y-AOs are used to improve N−H and N−C σ-bonding (sp instead of sp^2) and the π-bonding of N is not immediately affected. The nonplanar *N*-inversion transition state structure also contains only p_x-AO in its p_σ-lone pair and the p_y-AO again

dx.doi.org/10.1021/jo200411f |J. Org. Chem. 2011, 76, 3987–3996

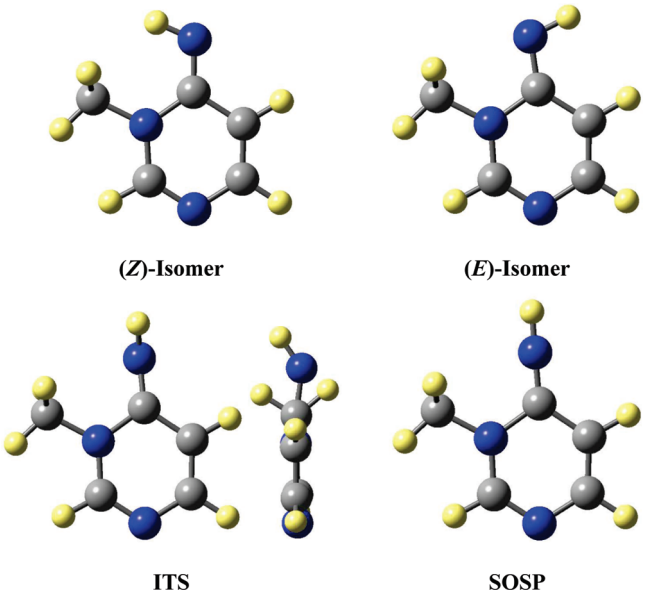

Figure 1. Molecular models of PCM optimized structures for 3-methyl-4-pyrimidine-(3*H*)-imine in the solvent heptane ($\varepsilon = 1.92$).

is used to improve N−H and N−C σ-bonding. However, the nonplanar *N*-inversion transition state structure employs only *some* of the s-AO to improve σ-bonding while the remainder of the s-AO at N is used to improve the (pseudo)-π-bonding. In the pure rotation process, the imine N_σ-lone pair retains its contributions from one s- and two p-AOs (contribution from p_y-AO is retained and the other p-contribution is a linear combination of the p_x- and p_z-AOs), and hence neither the N's σ-bonding nor its (pseudo)-π-bonding are improved. In such imines it might become advantageous to decrease the N's s-contributions to one or both of the N−H and N−C σ-bonds and to assume a sp^3-like N-hybridization.

In-plane and nonplanar imine-*N*-inversions, respectively, will occur in imines that offer opportunities for improved imine-N bonding in the isomerization transition state structure via the σ- or π-systems, respectively, and rotations occur otherwise. The present study exemplifies an imine for which nonplanar *N*-inversion offers stabilization in the (pseudo)-π-system.

Characteristic Structural Features. The molecular structures shown in Figure 1 of the (*E*)- and (*Z*)-minima, ITS, and SOSP of 3MePMI were optimized at the PCM level in heptane ($\varepsilon = 1.92$). These models are typical representatives of 3MePMI in various solvents. The CH_3 group is staggered with regard to the exocyclic imine bond in all stationary structures.

Key structural parameters for the characterization of the ITS and SOSP geometries determined at levels PCM and SMD are collected in Table 2. It is advantageous to describe the *N*-inversion of 3MePMI in terms of the angles α, β, η, and σ. The angle $\alpha = \angle(C{-}N{-}H)$ is the imine angle and the angle β is $\angle(X_C{-}N{-}H)$, where the dummy X_C is placed on the side of C_5 in the (N, C4, C5)-plane (Scheme 3). The displacement of the H-imine out of the (N, C4, C5)-plane is quantified by the dihedral angle, $\eta = \angle(H{-}N{-}X_C{-}C4)$. And finally, the dihedral angle $\sigma = \angle(N{-}C4{-}C5{-}N1)$ defines the displacement of the N-imine out of the (N1, C4, C5) plane ($\sigma \neq 180°$).

The (*E*)- and (*Z*)-minima exhibit α angles close to the sp^2 hybridization angle and the SOSP structures have α angles that

Table 2. *N*-Inversion Saddle Point Geometries Computed at Levels PCM and SMD

	ITS				SOSP
medium	α	β	η	σ	α
gas phase	140.69	93.81	140.59	−171.00	179.55
		PCM			
heptane	139.24	93.11	139.34	−170.88	179.95
chloroform	137.17	85.72	137.35	−170.56	179.43
methylene chloride	136.49	90.45	136.49	−170.66	179.26
water	134.24	93.64	134.83	−170.56	178.96
average[a]	136.46	91.06	136.53	−170.70	179.29
std dev[a]	1.40	2.62	1.40	0.21	0.31
		SMD			
heptane	137.54	92.42	137.59	−170.59	179.95
chloroform	134.50	94.23	134.65	−170.38	179.51
methylene chloride	132.87	93.12	132.95	−170.28	179.95
water	129.45	91.47	129.45	−170.50	179.03
average[a]	132.89	93.13	132.98	−170.35	179.44
std dev[a]	2.60	1.37	2.60	0.11	0.36

[a] Average and standard deviations based on all 14 solvents studied. See Supporting Information for complete version of this table.

Scheme 3. Atom Numbering and Definitions of Angles $\alpha = \angle(C{-}N{-}H)$ and $\beta = \angle(X_C{-}N{-}H)$

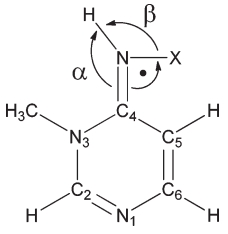

are very close to the sp hybridization angle. The ITS structures exhibit angles $\alpha = \angle(C{-}N{-}H)$ that are clearly larger than the sp^2 hybridization angle but are equally clearly well below 180°. The α values fall in the range 141−128°, and a significant inverse correlation exists between the imine angle α and solvent polarity ($\alpha(PCM) = -1.908 \ln(\varepsilon) + 140.5$, $R^2 = 0.9913$; $\alpha(SMD) = -2.447 \ln(\varepsilon) + 139.04$, $R^2 = 0.9404$).

The study of PMI showed that the *N*-inversion requires both the imine-H and the imine-N to move out of the best plane of the heterocycle and that the atoms move to opposite faces. The angles η and σ measure the degree of these out-of-plane (oop) motions and the sign difference in η and σ reflects their displacement in opposite directions. The β angle is 91 ± 3° in the ITS structures and hence $\eta \approx \alpha$ for both the PCM and SMD structures. The PCM and SMD data show that the imine-N displacement measure σ is essentially independent of solvent dielectric constant ($\sigma_{PCM} = -170.7 \pm 0.2°$; $\sigma_{SMD} = -170.4 \pm 0.1°$).

Solvation Effect on Isomer Preference Energies. The isomer preference energy for the (*E*)- over the (*Z*)-isomer is $\Delta E_r = 3.1$ kcal/mol at the MP2(full)/6-31G* level for PMI.[11] The steric demand of the CH_3 group increases the

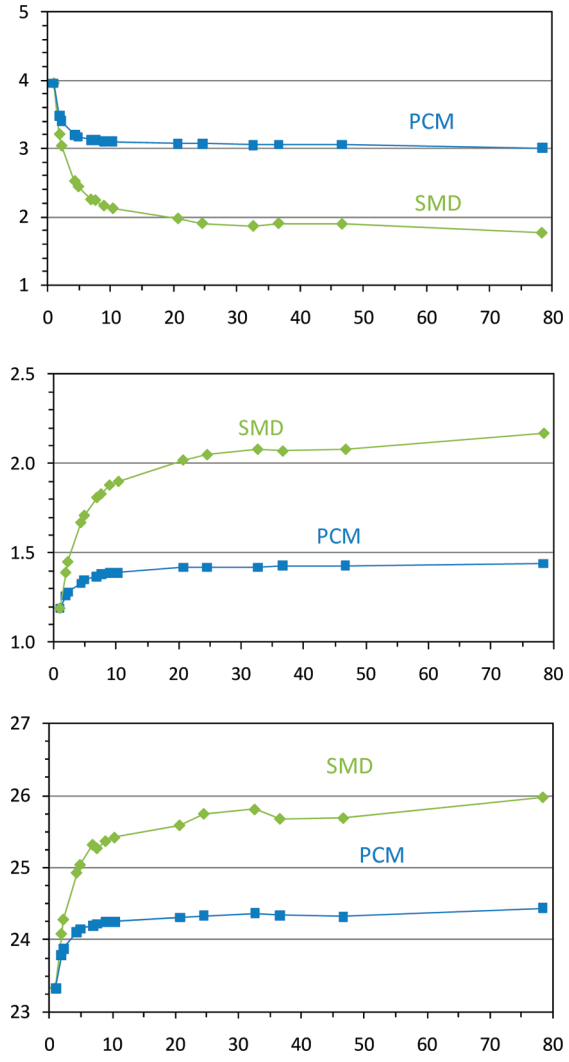

Figure 2. (a) Isomer preference energy (IPE, top), (b) asymmetrization energy ΔE_{def} (center), and (c) activation barrier E_{act} (bottom) as a function of solvent dielectric constant, ε. The blue and green curves show values computed for 14 solvents at levels PCM and SMD.

(*E*)-preference energy of 3MePMI to ΔE_r = 4.0 kcal/mol in the gas phase. The solvent models consistently predict a reduction of the isomer preference energy (IPE) of 3MePMI with increasing solvent polarity (Figure 2a), but there are significant differences regarding the magnitude and the steepness of the drop of IPE in the region of the low-polarity solvents. The PCM and SMD data suggest that IPE is sensitive to solvent polarity in the low-polarity region only and that any further increase of solvent polarity beyond $\varepsilon \approx 20$ would have only minor consequences on the isomer ratio. A similar conclusion was reached by a recent discussion of solvation energies of sulfanilamide at the PCM and the SMD levels.[26b]

The thermodynamic functions are essentially the same for the (*E*)- and (*Z*)-isomers and Table 1 shows that $\Delta E \approx \Delta G_{298}$ is an excellent approximation for the IPE values. For example, the gas-phase IPE values are ΔE = 3.96 and ΔG_{298} = 3.82 kcal/mol, and the IPE values in water are ΔE = 3.01 and ΔG_{298} = 3.09 kcal/mol (PCM) and ΔE = 1.76 and ΔG_{298} = 1.63 kcal/mol (SMD). While the solvent models consistently predict a reduction of the isomer preference energy of 3MePMI with increasing solvent polarity, the PCM and SMD methods predict solvation effects of significantly different size and suggest different outcomes in the laboratory. The PCM results suggest that the concentration of the (*Z*)-isomer is well below the NMR detection limit ($[(Z)]/[(E)] = 0.005$), whereas the SMD results predict the possibility of observation of both isomers ($[(Z)]/[(E)] = 0.063$).

Solvation Effect on Transition State Asymmetrization Energy. The most interesting parameter in the present context is the deformation energy $\Delta E_{def} = E(\text{SOSP}) - E(\text{ITS})$, that is, the preference for the nonplanar inversion transition state structure over its adjacent second-order saddle point structure. In the gas phase, the deformation energies ΔE_{def} are 0.9 kcal/mol for PMI[11] and 1.19 kcal/mol for 3MePMI. The solvation methods PCM and SMD both predict increases of ΔE_{def} for 3MePMI with increasing solvent polarity (Figure 2b), and the ΔE_{def} values computed for water are 1.44 kcal/mol (PCM) and 2.17 kcal/mol (SMD), respectively.

The approximation $\Delta E \approx \Delta G_{298}$ holds well for the relative isomer stabilities IPE because both isomers have the same number and types of internal degrees of freedom. For the deformation energies E_{def}, on the other hand, the ΔG_{298} values are lower than the ΔE values because the thermal energy of the transition state structures includes the contribution of one more vibrational mode. This difference is exaggerated because the second imaginary mode computed for the SOSP structure in the local approximation corresponds to a real mode in a nonlocal approximation, which correctly reflects the double-minimum shape of the potential energy surface in that dimension. Therefore, the ΔG_{298} values computed with the local approximation are lower bounds and their values ΔG_{298}(gas) = 0.70 kcal/mol, ΔG_{298}(water, PCM) = 0.84 kcal/mol, and ΔG_{298}(water, SMD) = 1.22 kcal/mol corroborate the relation of E_{def}(gas) < E_{def}(solvent) < E_{def}(polar solvent).

Solvation Effect on *N*-Inversion Activation Barriers. We showed previously by population analysis that the exocyclic C═NH moiety of pyrimidine-4(3*H*)-imine, PMI, is highly polarized and that the isomerization requires additional polarization of the already highly polar imine bond, and we argued that this fact is the fundamental origin of the isomerization barrier.[11] An increase of bond polarity along the path from substrate to transition state usually is associated with a positive solvent effect, that is, the activation barrier decreases with an increase in solvent polarity. Considering the increase of the bond polarity of the C═NH moiety during *N*-inversion, one might expect a positive solvent effect. Yet, the plots of $E_{act} = f(\varepsilon)$ in Figure 2c clearly show a *negative* solvent effect on the *N*-inversion barrier, that is, the activation barrier of the C═NH polarity-increasing isomerization process *increases* with solvent polarity. The values computed with both solvation models all exceed the computed gas-phase barrier of E_{act} = 23.3 kcal/mol, and the $E_{act}(H_2O)$ values are 24.4 (PCM) and 26.0 kcal/mol (SMD), respectively.

For the activation energies E_{act}, the ΔG_{298} values are about 2.0 ± 0.2 kcal/mol below the ΔE values because the thermal energy of the isomer includes the contribution of one more vibrational mode than the thermal energy of the transition state structure. The ΔG_{298} value of the computed gas-phase barrier is 21.5 kcal/mol, and the respective values computed for aqueous solution are 22.1 (PCM) and 23.8 kcal/mol (SMD), respectively.

Charge Distributions and C═NH Polarity Enhancement in Solution. The charge distributions (NBO[29]) were computed for the stationary structures of 3-methyl-4-pyrimidine-(3*H*)-imine of the free molecule and in solution, and the results are provided

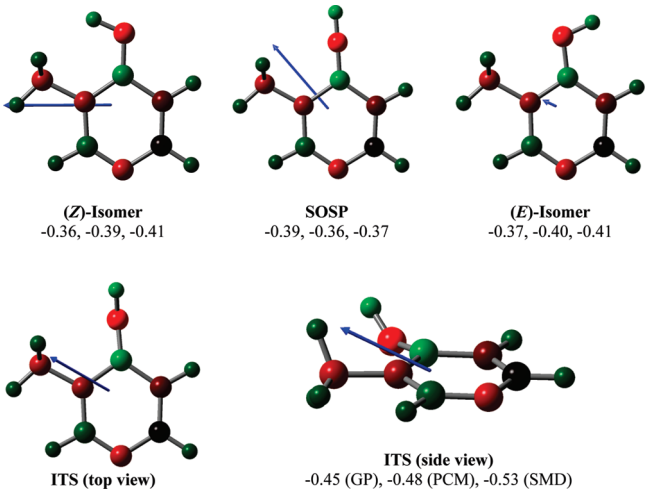

Figure 3. Charge distribution (NBO) and molecular dipole moments of the MP2(full)/6-31G* optimized stationary structures for 3-methyl-4-pyrimidine-(3*H*)-imine. Charge distribution indicated by color from red (−0.85) to green (+0.85). NBO charges provided for the NH group computed for the free molecule and with the PCM and SMD methods for aqueous solution.

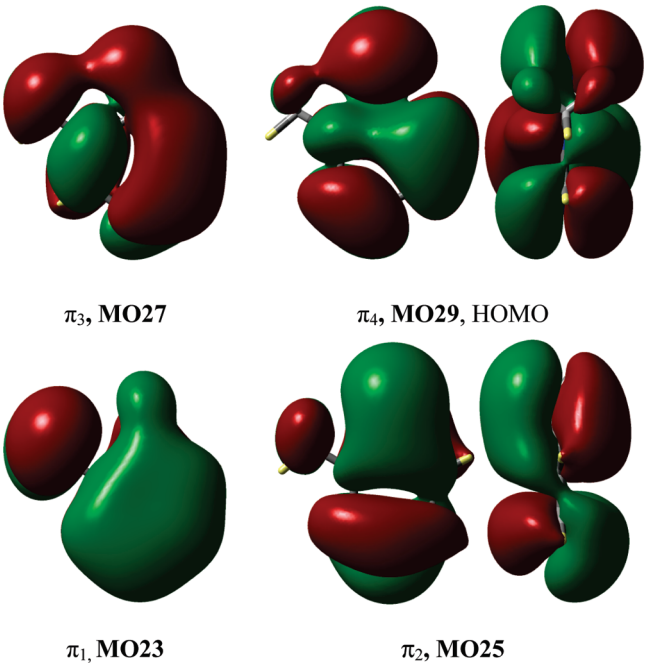

Figure 4. Surface plots of the pseudo-π-MOs of the ITS structure of 3-methyl-4-pyrimidin-(3*H*)-imine: MO23, MO25, MO27, and MO29 (HOMO).

as Supporting Information (Table S5). The gas-phase charge distributions are illustrated in Figure 3 by the coloring scheme, and they are very similar to the parent system PMI. The NH group always carries negative charge and the absolute values of the charges follow the order $|q^{NH}(E)| \approx |q^{NH}(Z)| < |q^{NH}(SOSP)| < |q^{NH}(ITS)|$ in the gas phase. Solvation increases the NH group charge of the isomers and especially of the ITS structure but reduces the value for the SOSP structure, and hence the ordering in solution becomes $|q^{NH}(SOSP)| < |q^{NH}(E)| \approx |q^{NH}(Z)| < |q^{NH}(ITS)|$.

The key to understanding *N*-inversion in 4-pyrimidinimine is the recognition that the HOMO (π_4) is formed by the antibonding combination of the NH group's p_π-type FMO and the pyrimidine π_3-type MO, and hence the π-interaction in the HOMO is repulsive in the region of the exocyclic C═N bond. We showed for the parent 4-pyrimidinimine that the out-of-plane deformation of the imine moiety does have a significant effect on the HOMO in that it creates two additional overlaps between lopes on opposite faces of the best plane of the heterocycle: major overlap occurs between the imine-N and N3 (primary overlap) and a smaller (secondary) overlap occurs between N3 and C2.[11] Based on this observation, we argued that the oop-deformation allows for more delocalization of electron density (without any need for intramolecular charge transfer) and the extra-stabilization of the nonplanar ITS structure by this effect should be most effective when the dihedral angles η and σ are out-of-phase. The argument holds for the N-methyl derivative.

The four pseudo-π-MOs of 3-methyl-4-pyrimidineimine are shown in Figure 4. The π-type CH_3 group orbital is antibonding in the N3−CH_3 region in all four pseudo-π-MOs, and interestingly, molecular orbitals π_3 and π_4 feature overlap between the methyl group and the exocyclic imine-N. Three of the four pseudo-π-MOs are bonding in the region of the exocyclic C═N bond. The HOMO, π_4 is antibonding in that region in the SOSP structure and the oop-deformation of 3MePMI is required to create two additional, stabilizing overlaps between lobes on opposite faces of the best plane of the heterocycle. MO29 features major, primary overlap between the imine-N and N3 and a smaller, secondary overlap occurs between N3 and C2. Solvation can enhance this HOMO stabilization mechanism by providing additional incentive to transform the p_π-type lone pair density at N toward a sp^x-shaped lone pair density.

The (NH, pyrimidine)-overlaps in MO23, MO25, and MO27 intrinsically benefit from the p_π-shape of the lone pair density of the imine-N; these overlaps favor planar *N*-inversion and resist the oop-deformation. The exocyclic bond length of the SOSP structure is shorter than in the isomers (*E*: 1.294 Å; *Z*: 1.293, SOSP: 1.244; ITS: 1.266) because of the changed N-hybridization (sp^2 to sp) and despite the increased repulsion this causes in the HOMO (which has a node in the CN bonding region). In the SOSP structure, this repulsion in the HOMO is reduced by HN → pyrimidine charge transfer within $\pi_1-\pi_3$, and this mechanism is manifest in the relation of the NH group charges $|q^{NH}(SOSP)| < |q^{NH}(ITS)|$.

Molecular Dipole Moments and the N-Lone Pair Dipole Moment. The solvent effects on the atomic charges are modest, and the molecular dipole moments are superior indicators of changes to the electron density distribution in the imine-N basins. The dipole moments of the free (*Z*)- and (*E*)-isomers are 3.27 and 0.45 D, respectively, and the dipole moments of the ITS and SOSP structures are 2.32 and 2.76 D, respectively. The dipole moment vectors shown in Figure 3 are directed from the negative to the positive pole.

The molecular dipole moments μ computed for each stationary structure for every solvent in our set are provided in Supporting Information (Table S6), and Figure 5 provides perspective. Both solvent models consistently predict the ordering $\mu(E) \ll \mu(ITS) < \mu(SOSP) < \mu(Z)$, both models predict increases in the molecular dipole moments of every stationary structure with increasing solvent polarity, and both models feature steep

Scheme 4. Determination of Dipole vectors $\mu(N_{lp}, Z) = \mu(Z) - \mu(SOSP)$, $\mu(N_{lp}, E) = \mu(E) - \mu(SOSP)$, and $\mu(N_{lp}, ITS) = \mu(ITS) - \mu(SOSP)$ and Their Interpretation as N-Lone Pair Dipoles

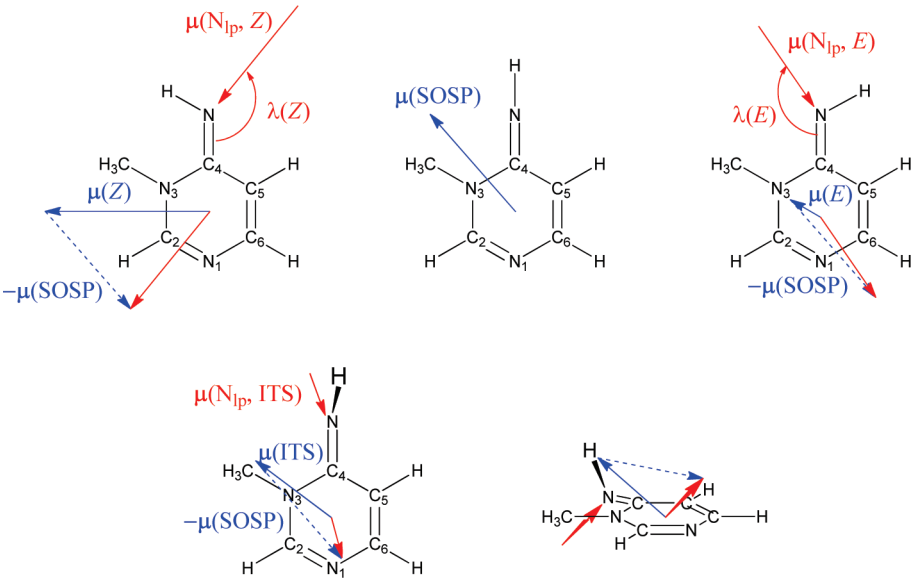

Table 3. Computed *N*-Lone Pair Dipole Moments: Magnitude and Directions at the SMD Level

medium	ε	$\lvert\mu(N_{lp}, Z)\rvert$	$\lambda(Z)$	$\lvert\mu(N_{lp}, E)\rvert$	$\lambda(E)$	$\langle\mu(N_{lp})\rangle$	$\Delta\mu(N_{lp})$	$\mu(N_{lp}, ITS)$	$\lambda(ITS)$	$\omega(ITS)$
gas phase	1	2.813	145.19	2.347	146.66	2.580	0.466	1.583	137.01	27.64
heptane	1.92	3.152	144.83	2.632	147.61	2.892	0.520	1.984	141.23	29.27
benzene	2.25	3.203	144.78	2.699	147.74	2.951	0.504	2.094	142.14	29.70
diethyl ether	4.34	3.442	144.42	2.908	147.97	3.175	0.534	2.480	144.75	31.17
chloroform	4.90	3.470	144.35	2.935	147.97	3.203	0.535	2.540	145.07	31.38
aniline	6.89	3.557	144.13	3.018	148.00	3.288	0.539	2.730	146.04	32.02
THF	7.58	3.567	144.13	3.034	148.00	3.301	0.533	2.755	146.19	32.05
methylene chloride	8.93	3.597	144.06	3.064	147.98	3.331	0.533	2.831	146.55	32.24
dichloroethane	10.36	3.620	144.01	3.083	147.99	3.352	0.537	2.874	146.76	32.35
acetone	20.70	3.690	143.81	3.157	147.97	3.424	0.533	3.067	147.59	32.79
ethanol	24.55	3.700	143.74	3.168	147.97	3.434	0.532	3.146	147.90	33.03
methanol	32.63	3.713	143.70	3.183	147.96	3.448	0.530	3.203	148.13	33.16
acetonitrile	36.64	3.720	143.73	3.190	147.96	3.455	0.530	3.162	147.98	32.98
DMSO	46.70	3.731	143.68	3.201	147.98	3.466	0.530	3.182	148.04	33.01
water	78.39	3.734	143.55	3.210	147.88	3.472	0.524	3.365	148.77	33.52

dipole increases in the low-ε region except for the (*E*)-isomer. The ordering and solvent dependence of the molecular dipoles are in line with the solvation effects on the isomer preference energy IPE and the activation energy $E_{act}(Z \rightarrow ITS)$.

A much better appreciation of the relaxation of the electronic structure along the *N*-inversion path is achieved by analysis of the dipole moments relative to the SOSP structure. We define $\mu(N_{lp}, Z) = \mu(Z) - \mu(SOSP)$, $\mu(N_{lp}, E) = \mu(E) - \mu(SOSP)$, and $\mu(N_{lp}, ITS) = \mu(ITS) - \mu(SOSP)$ and recognize and interpret the resulting vectors as *N*-lone pair dipole moment vectors. The dipole moments $\mu(N_{lp})$ are directed from the center of the lone pair region to the position of the imine-N. The SOSP structure is special in that it lacks an N-lone pair. Starting with the molecular dipole moment of the SOSP structure, the contribution of $\mu(N_{lp})$ increases or decreases the magnitude of the molecular dipole moments of the (*Z*)- and (*E*)-isomers and changes their directions as expected on the basis of vector addition (Scheme 4).

To determine $\mu(N_{lp}, Z)$, $\mu(N_{lp}, E)$ and $\mu(N_{lp}, ITS)$, the respective structure was realigned with the SOSP structure so that the imine CN bonds were parallel and that the structures were coplanar and had the same two-dimensional chirality.[30] The lengths of the resulting dipoles $\mu(N_{lp}, Z)$ and $\mu(N_{lp}, E)$ are listed in Table 3 together with the angles $\lambda(Z)$ and $\lambda(E)$ they enclose with the imine CN direction (Scheme 4). The N-lone pair dipole moment of the transition state structure ITS is determined in analogy, and the direction of $\mu(N_{lp}, ITS)$ is specified by the angles $\lambda(ITS)$ and $\omega(ITS)$ enclosed with the imine CN direction and measured in the molecular plane or perpendicular to the molecular plane, respectively.

Solvent Stabilization of N-Lone Pair Density. The plots in Figure 6 reveal that the variation of the molecular dipole

dx.doi.org/10.1021/jo200411f |*J. Org. Chem.* 2011, 76, 3987–3996

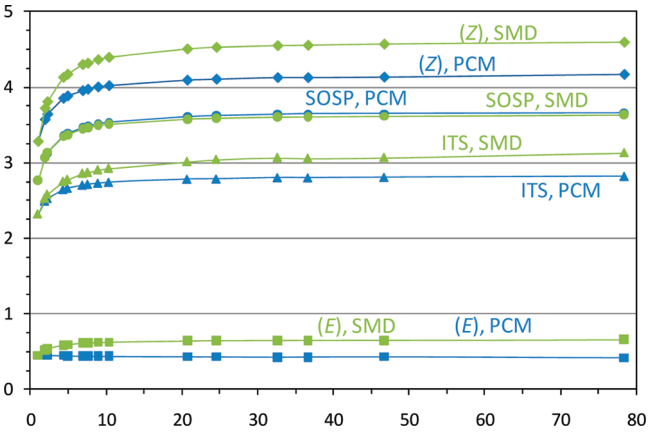

Figure 5. Molecular dipole moment, μ, of stationary structures as a function of solvent dielectric constant, ε. The blue and green curves, respectively, represent dipole moments computed for 14 solvents at the PCM and SMD levels, respectively. (◆) (*Z*)-Isomer; (■) (*E*)-Isomer; (▲) ITS; (●) SOSP.

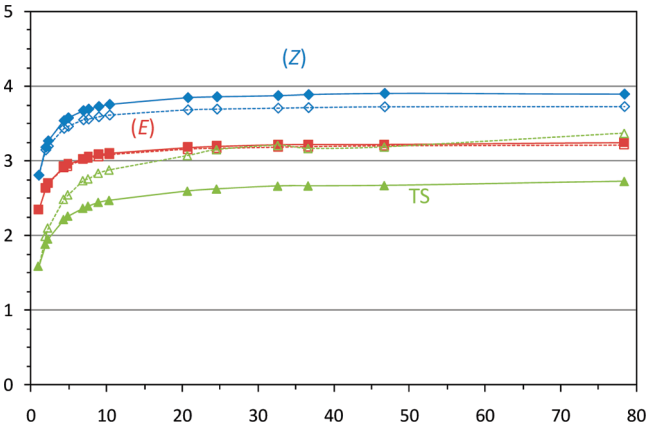

Figure 6. N-Lone pair dipole moments $\mu(N_{lp}, Z)$, $\mu(N_{lp}, E)$, and $\mu(N_{lp}, ITS)$ as a function of solvent dielectric constant, ε. Data for (*Z*)-isomer shown as blue diamonds, for (*E*)-isomer as red squares, and for ITS as green triangles. The solid and dashed curves represent dipole moments computed at the PCM and SMD levels.

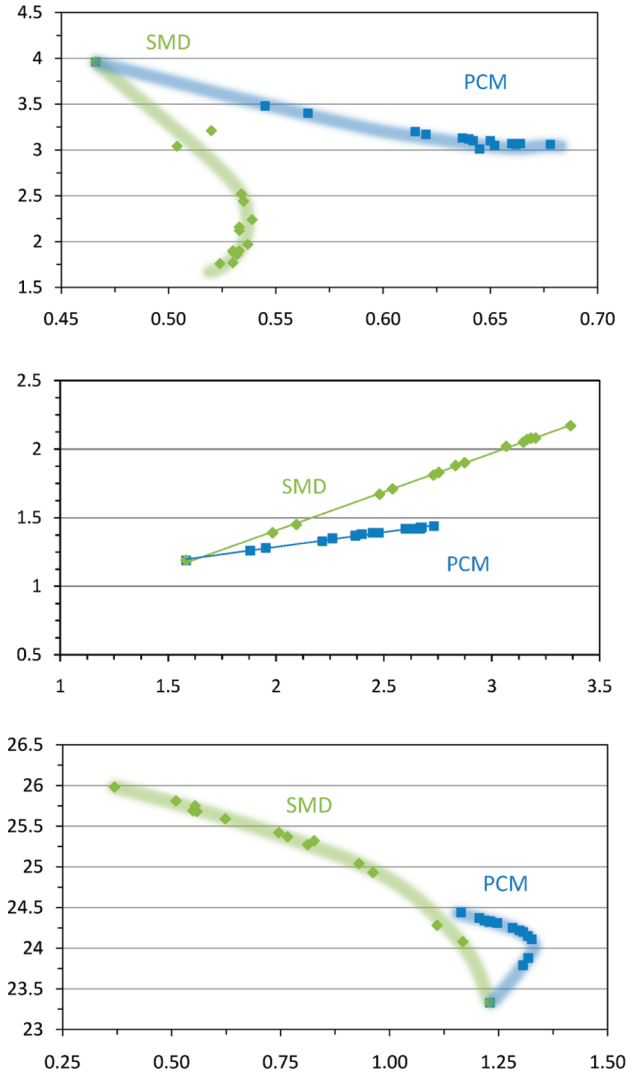

Figure 7. From top to bottom, the graphs show (a) the isomer preference energy as a function of the dipole difference $\Delta\mu_{iso} = \mu(N_{lp}, Z) - \mu(N_{lp}, E)$, (b) the deformation energy as a function of the dipole moment $\mu(N_{lp}, ITS)$, and (c) the activation energy as a function of the dipole difference $\Delta\mu_{act} = \mu(N_{lp}, Z) - \mu(N_{lp}, ITS)$. The blue and green curves show data computed at PCM and SMD, respectively.

moments is dominated by the contribution $\mu(N_{lp})$ of the imine-N's lone pair. The variation of $\mu(N_{lp})$ as a function of solvent polarity is conceptually reasonable in that both $\mu(N_{lp}, Z)$ and $\mu(N_{lp}, E)$ increase with increasing solvent polarity. The plots in Figure 6 show that $\mu(N_{lp}, E) < \mu(N_{lp}, Z)$ in all media. The gas-phase values are $\mu(N_{lp}, E) = 2.35$ D and $\mu(N_{lp}, Z) = 2.81$ D, and they increase by some 35−40% in aqueous solution (PCM: $\mu(N_{lp}, E) = 3.25$ D, $\mu(N_{lp}, Z) = 3.90$ D; SMD: $\mu(N_{lp}, E) = 3.20$ D, $\mu(N_{lp}, Z) = 3.73$ D). Importantly, the analysis shows (a) that the nonplanar *N*-inversion transition state structure allows for a substantial *N*-lone pair dipole moment of $\mu(N_{lp}, ITS) = 1.58$ D in the gas phase and (b) that $\mu(N_{lp}, ITS)$ increases in aqueous solution (PCM: $\mu(N_{lp}, ITS) = 2.73$ D (+73%); SMD: $\mu(N_{lp}, ITS) = 3.37$ D (+113%)) roughly twice as much as the one of either isomer.

The $\lambda(E)$ angles fall in a narrow range of 147.5 ± 1.0° for all media and independently of the solvent model and the $\lambda(Z)$ angles are about 1.5−4° smaller with a minor effect of the medium (GP, PCM: 1.5−2°; SMD: 3−4°). The $\lambda(ITS)$ angle is 137.0° in the gas phase, its value increases in solution and the increase correlates with solvent polarity (PCM: 140−145°; SMD: 141−149°). In gas phase the ∠(H−N−C) angles of the isomers are $\alpha(E) = 109.0°$ and $\alpha(Z) = 112.6°$, respectively. Assuming to a first approximation that the lone pair is collinear with the α bisector, these α angles suggest $\lambda'(E) = 125.5°$ and $\lambda'(Z) = 123.7°$. While the relation $\lambda(E) > \lambda(Z)$ is as expected, the actual λ angles exceed the λ' values by some 22° in the direction suggested by VSEPR concepts.[31] Also in the gas phase, the ∠(H−N−C) angle of the inversion transition state structure is $\alpha(ITS) = 140.7°$, and hence $\lambda(ITS) = 137.0°$ exceeds $\lambda'(ITS) = 109.6°$ by some 27° and significantly more than in the isomers.

There exists a strong inverse correlation between the solvent effect on $\lambda(ITS)$ and the associated variation of $\alpha(ITS)$. One would expect roughly that $\Delta\alpha(ITS) + 2\Delta\lambda(ITS) \approx 0$ assuming that the change of the lone pair direction would track the change of the direction of the α bisector. However, it is found that the value of $\Delta\alpha(ITS) + 2\Delta\lambda(ITS)$ very quickly rises in solution to

dx.doi.org/10.1021/jo200411f |*J. Org. Chem.* 2011, 76, 3987–3996

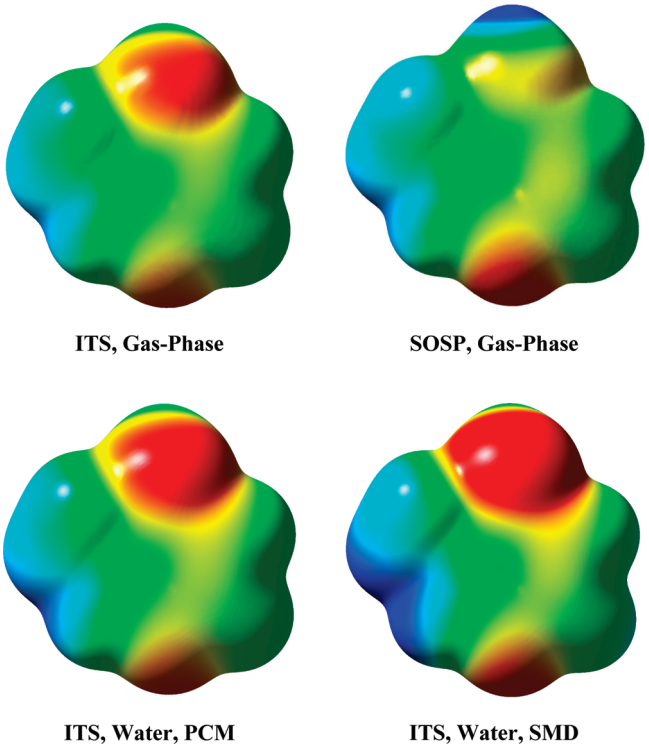

Figure 8. Electrostatic potential plots of the ITS and SOSP structures of 3-methyl-4-pyrimidin-imine in the gas phase (top) and of the ITS structure in aqueous solution as simulated using the PCM and SMD models. In all cases, the electrostatic potential (−0.05 (red) to +0.05 (blue)) is mapped on the isosurface of the total electron density (ρ_{iso} = 0.001 e/au^{-3}) computed at the same level.

approach ∼10° (PCM) or ∼12° (SMD). In fact, for media with a dielectric constant $\varepsilon > 10$ the relation $\Delta\alpha(\mathrm{ITS}) \approx -\Delta\lambda(\mathrm{ITS})$ fits the data much more closely than $\Delta\alpha(\mathrm{ITS}) = -2\Delta\lambda(\mathrm{ITS})$. Consequently, $\lambda(\mathrm{ITS})_{sol}$ exceeds $\lambda'(\mathrm{ITS})_{sol}$ by even more than 27°, and specifically $\lambda(\mathrm{ITS})_{aq,PCM}$ = 144.8° exceeds $\lambda'(\mathrm{ITS})_{aq,PCM}$ = 112.6° by 32.2° and $\lambda(\mathrm{ITS})_{aq,SMD}$ = 148.8° exceeds $\lambda'(\mathrm{ITS})_{aq,SMD}$ = 115.2° by 33.6°.z

N-Lone Pair Moments and Energy Parameters. With increasing solvent polarity, the solvation models consistently predict a reduction of the isomer preference energy (IPE) of 3MePMI (Figure 2a), an increase of the asymmetrization energy E_{def} (Figure 2b), and an increase of E_{act} (Figure 2c). We can now examine the relations between the values of IPE, E_{def}, and E_{act} and the *N*-lone pair dipole moments (Figure 7).

The plots of the deformation energies (Figure 7, center) as a function of the dipole moments $\mu(N_{lp}, \mathrm{ITS})$ show a stunning fit of the computed data by the linear regression functions E_{def}(PCM) = 0.2152 $\mu(N_{lp}, \mathrm{ITS})$ + 0.8566 (R^2 = 0.9946) and E_{def}(SMD) = 0.5628 $\mu(N_{lp}, \mathrm{ITS})$ + 0.2817 (R^2 = 0.9992). This correlation provides strong evidence in support of our thesis that solvation enhances the HOMO stabilization mechanism by providing additional incentive to orient and to spatially extend the *N*-lone pair density. The transformation of the p_π-type lone pair density at N toward an sp^x-shaped lone pair in going from the SOSP structure of the in-plane *N*-inversion to the ITS structure of the asymmetric path is clearly visible in the more negative electrostatic potential in the imine-N's lone pair density region in the ITS structure as compared to the respective region of the SOSP structure (Figure 8, top). The surface plots of the electrostatic potential[32] computed with the PCM and SMD electron densities (Figure 8, bottom) for aqueous solution exemplify that solvation greatly enhances the HOMO stabilization mechanism.

The plots of the isomer preference energies (Figure 7, top) and the activation energies (Figure 7, bottom) as functions of the dipole moment changes $\Delta\mu_{iso}$ and $\Delta\mu_{act}$, respectively, show no simple correlations, and the shapes of the curves are qualitatively different for the two solvation models. The linear correlation of E_{def} with $\mu(N_{lp}, \mathrm{ITS})$ is successful because the electronic structures of SOSP and ITS are rather similar to begin with, and because of their similarity, the local effect at the imine-N can make the difference. On the other hand, the IPE and E_{act} values depend on two structures that are intrinsically rather different, and one local feature may not dominate the overall solvent effect and may even go in the opposite direction. Solvent does enhance the N-lone pair in the ITS structure, $\mu(N_{lp}, \mathrm{ITS})$ does grow more than $\mu(N_{lp}, Z)$ with increasing solvent polarity, and yet the activation barrier for the $(Z) \rightarrow (E)$ isomerization goes up with solvent polarity because of the differences in the molecular dipole moments (Figure 5, $\mu(\mathrm{ITS}) < \mu(Z)$).

CONCLUSION

The (*E*)-isomer preference energy of 3MePMI in the gas phase is ΔG_{298} = 3.8 kcal/mol and the gas-phase activation barrier $E_{act}(Z \rightarrow E)$ is ΔG_{298} = 21.5 kcal/mol. The solvent models consistently predict a reduction of the (*E*)-isomer preference energy of 3MePMI and an increase of the activation barrier $E_{act}(Z \rightarrow E)$ with increasing solvent polarity. Short-range solvent structural effects (CDS) should play an important role for pyrimidines, and these are considered in the SMD data. The SMD data computed for aqueous solution predict an IPE value of ΔG_{298} = 1.6 kcal/mol and an $E_{act}(H_2O)$ value of ΔG_{298} = 23.8 kcal/mol. Hence, the results suggest that both isomers should be observable by NMR spectroscopy and that the thermal isomerization can be studied by variable-temperature NMR methods.

The (*E*)/(*Z*)-isomerizations of 4-pyrimidin-(3*H*)-imine PMI and of 3-methyl-4-pyrimidinimine 3MePMI proceed via asymmetric imine *N*-inversion. The HOMO in 4-pyrimidin-(3*H*)-imine (π_4) is antibonding in the region of the exocyclic C═NH bond. The out-of-plane deformation of the imine moiety, characterized by out-of-phase dihedral angles η and σ, allows for additional delocalization of electron density in the HOMO of the transition state structures for nonplanar *N*-inversion without any need for intramolecular charge transfer. The nonplanarity of the *N*-inversion in 4-pyrimidin-(3*H*)-imines is intrinsic, and we expect asymmetric *N*-inversion paths to occur quite generally in heteroarene imines of this type (i.e., derivatives of pyridin-2(1*H*)-imines, 2*H*-pyran-2-imine, etc.).

The enantiomeric paths for nonplanar *N*-inversion show that the potential energy surface in the isomerization region between the (*E*)- and (*Z*)-imines features a double-valley between bifurcation and convergence regions and it is expected that the isomerization trajectories will fall into two bundles.

The asymmetrization of the *N*-inversion can be enhanced by extrinsic factors that stabilize the evolving N-lone pair at the imine-N. The results of the present study show that general solvation increases the dipole moment $\mu(N_{lp}, \mathrm{ITS})$ associated with the imine group's N-lone pair, that $\mu(N_{lp}, \mathrm{ITS})$ increases with solvent polarity, and that the deformation energies E_{def} are linearly correlated to the dipole moment $\mu(N_{lp}, \mathrm{ITS})$.

Isomerization of 4-pyrimidine-(3*H*)-imines requires additional polarization of the already very polar C═NH bond, and this is the fundamental origin of the isomerization barrier. Solvents of increasing polarity facilitate the additional polarization of the exocyclic C═N bond as well as the formation of the dipole moment $\mu(N_{lp}$, ITS), and yet the present study clearly shows a *negative* solvent effect on the *N*-inversion barrier ($E_{act} = f(\varepsilon)$ in Figure 2), that is, the activation barrier increases with solvent polarity. This situation arises because the increase in the *local* polarity of the exocyclic imine moiety causes a reduction of the solute's overall *molecular* dipole moment.

■ ASSOCIATED CONTENT

Supporting Information. Tables of total energies, thermodynamic data, relative isomer stabilities and activation energies, results of population analysis, molecular dipole moments, and Cartesian coordinates of stationary structures optimized for 3-methyl-4-pyrimidinimine in all media at levels PCM and SMD. This material is available free of charge via the Internet at http://pubs.acs.org.

■ AUTHOR INFORMATION

Corresponding Author
*E-mail: glaserr@missouri.edu.

■ REFERENCES

(1) For acid-catalyzed imine inversion, see for example: Johnson, J.; Morales, N.; Gorczyca, A.; Dolliver, D.; McAllister, M. *J. Org. Chem.* **2001**, *66*, 7979–7985.

(2) For base-catalyzed imine inversion with deprotonation of imine-R, see for example: Cainelli, G.; Giacomini, D.; Trerè, A.; Boyl, P. *J. Org. Chem.* **1996**, *61*, 5134–5139.

(3) For base-catalyzed imine inversion with deprotonation at C_α, see for example: Gosselin, F.; Roy, A.; O'Shea, P.; Chen, C.; Volante, R. *Org. Lett.* **2004**, *6*, 641–644.

(4) (a) Curtin, D.; Hausser, J. *J. Am. Chem. Soc.* **1961**, *83*, 3474–3481. (b) Curtin, D. Y.; Grubbs, E. J.; McCarty, C. G. *J. Am. Chem. Soc.* **1966**, *88*, 2775–2786.

(5) Jennings, W.; Al-Showiman, S.; Boyd, D.; Campbell, R. *J. Chem. Soc., Perkin Trans. II* **1976**, 1501–1506.

(6) Reich, B.; Greenwald, E. E.; Justice, K. A.; Beckstead, B. T.; Reibenspies, J. H.; North, W. S.; Miller, S. A. *J. Org. Chem.* **2005**, *70*, 8409–8416.

(7) (a) Bach, R. D.; Wolber, G. J. *J. Org. Chem.* **1982**, *47*, 245–248. (b) Bach, R. D.; Wolber, G. J. *J. Org. Chem.* **1982**, *47*, 239–245.

(8) Gálvex, J.; Guirado, A. *J. Comput. Chem.* **2010**, *31*, 520–531.

(9) Öğretir, C.; Yaman, M. *THEOCHEM* **1999**, *458*, 217–226.

(10) Smets, J.; Adamowicz, L.; Maes., G. *J. Phys. Chem.* **1995**, *99*, 6387–6400.

(11) Glaser, R.; Yin, J.; Miller, S. *J. Org. Chem.* **2010**, *75*, 1132–1142.

(12) Hernandez-Trujillo, J.; Bader, R. F. W. *J. Phys. Chem. A* **2000**, *104*, 1779–1794.

(13) (a) Trinajstic, N. *Croat. Chem. Acta* **1966**, *38*, 287–289. (b) Fayet, J. P.; Mauret, P. *J. Chim. Phys. Phys.-Chim. Biol.* **1971**, *68*, 156–158.

(14) (a) Osawa, E.; Yoshida, Z. *Spectrochim. Acta A* **1967**, *23*, 2029–2036. (b) Maijs, L.; Fainshtein, G. N. *Latv. PSR Zinat. Akad. Vestis, Kim. Ser.* **1976**, *5*, 593–594. (c) Podkovyrina, N. S.; Kataeva, L. M. *Sb. Aspir. Rab.-Kazan. Gos. Univ. im. V. I. Ul'yanova-Lenina, Estestv. Nauki, Khim.* **1973**, 11–18.

(15) (a) Poole, C. F.; Poole, S. K. *J. Chromatogr. A* **2002**, *965*, 263–299. (b) Poole, C. F.; Li, Q.; Kiridena, W.; Koziol, W. W. *J. Chromatogr. A* **2001**, *912*, 107–117.

(16) Lee, Y.-C.; Curtiss, L. A.; Ratner, M. A.; Shriver, D. F. *J. Phys. Chem. B* **1999**, *103*, 6445–6449.

(17) (a) Glaser, R.; Sui, Y.; Sarkar, U.; Gates, K. *J. Phys. Chem. A* **2008**, *112*, 4800–4814. (b) Smit, W. M. A.; Van Dam, T. *J. Chem. Phys.* **1980**, *72*, 3658–3662. (c) Glaser, R.; Chen, S. G. *Chem. Mater.* **1997**, *9*, 28–35.

(18) Cramer, C. J. *Essentials of Computational Chemistry*; Wiley: New York, NY, 2004.

(19) Pople, J. A. *Rev. Modern Phys.* **1999**, *71*, 1267–1274.

(20) Wilson, S. *Handb. Mol. Phys. Quantum Chem.* **2003**, *2*, 314–373.

(21) Hehre, W. J.; Ditchfield, R.; Pople, J. A. *J. Chem. Phys.* **1972**, *56*, 2257–2261.

(22) (a) Wahlin, P.; Schimmelpfennig, B.; Wahlgren, U.; Grenthe, I.; Vallet, V. *Theo. Chem. Acc.* **2009**, *124*, 377–384. (b) Kongsted, J.; Mennucci, B. *J. Phys. Chem. A* **2007**, *111*, 9890–9900.(c) Jensen, L.; van Duijnen, P. Th. The discrete solvent reaction field model: A quantum mechanics/molecular mechanics model for calculating nonlinear optical properties of molecules in condensed phase. In *Atoms, Molecules and Clusters in Electric Fields. Theoretical Approaches to the Calculation of Electric Polarizability*, 1st ed.; Maroulis, G., Ed.; Imperial College Press: London, 2006; pp 283−325.

(23) (a) Cancès, E.; Mennucci, B.; Tomasi, J. *J. Chem. Phys.* **1997**, *107*, 3032–3041.

(24) (a) Tomasi, J.; Cappelli, C.; Mennucci, B.; Cammi, R. From molecular electrostatic potentials to solvation models and ending with biomolecular photophysical processes. In *Quantum Biochemistry*, 1st ed.; Matta, C. F., Ed.; Wiley-VCH: Weinheim, Germany, 2010; pp 131−170. (b) Tomasi, J. Modern theories of continuum models: The physical model. In *Continuum Solvation Models in Chemical Physics: From Theory to Application*, 1st ed.; Mennucci, B., Cammi, R., Eds.; John Wiley & Sons Ltd.: West Sussex, 2007; pp 1−28.

(25) (a) Ribeiro, R. F.; Marenich, A. V.; Cramer, C. J.; Truhlar, D. G. *J. Comput.-Aided Mater.* **2010**, *24*, 317–333. (b) Marenich, A. V.; Cramer, C. J.; Truhlar, D. G. *J. Phys. Chem. B* **2009**, *113*, 6378–6396.

(26) (a) Marenich, A. V.; Cramer, C. J.; Truhlar, D. G. *J. Phys. Chem. B* **2009**, *113*, 4538–4543. (b) Halim, M. A.; Shaw, D. M.; Poirier, R. A. *THEOCHEM* **2010**, *960*, 63–72. (c) Saielli, G. *J. Phys. Chem. A* **2010**, *114*, 7261–7265.

(27) Frisch, M. J.; Trucks, G. W.; Schlegel, H. B.; Scuseria, G. E.; Robb, M. A.; Cheeseman, J. R.; Scalmani, G.; Barone, V.; Mennucci, B.; Petersson, G. A; Nakatsuji, H.; Caricato, M.; Li, X.; Hratchian, H. P.; Izmaylov, A. F.; Bloino, J.; Zheng, G.; Sonnenberg, J. L.; Hada, M.; Ehara, M.; Toyota, K.; Fukuda, R.; Hasegawa, J.; Ishida, M.; Nakajima, T.; Honda, Y.; Kitao, O.; Nakai, H.; Vreven, T.; Montgomery, Jr., J. A.; Peralta, J. E.; Ogliaro, F.; Bearpark, M.; Heyd, J. J.; Brothers, E.; Kudin, K. N.; Staroverov, V. N.; Kobayashi, R.; Normand, J.; Raghavachari, K.; Rendell, A.; Burant, J. C.; Iyengar, S. S.; Tomasi, J.; Cossi, M.; Rega, N.; Millam, N. J.; Klene, M.; Knox, J. E.; Cross, J. B.; Bakken, V.; Adamo, C.; Jaramillo, J.; Gomperts, R.; Stratmann, R. E.; Yazyev, O.; Austin, A. J.; Cammi, R.; Pomelli, C.; Ochterski, J. W.; Martin, R. L.; Morokuma, K.; Zakrzewski, V. G.; Voth, G. A.; Salvador, P.; Dannenberg, J. J.; Dapprich, S.; Daniels, A. D.; Farkas, Ö.; Foresman, J. B.; Ortiz, J. V.; Cioslowski, J.; and Fox, D. J. *Gaussian 09, Rev. A.1*; Gaussian, Inc.: Wallingford, CT, 2009.

(28) Dennington, R.; Keith, T.; Millam, J. *GaussView 5.0.8*; Semichem Inc.: Shawnee Mission, KS, 2009.

(29) (a) Weinhold, F. Natural bond orbital methods. In *Encyclopedia of Computational Chemistry*; Schleyer, P. v. R., Allinger, N. L.;, Clark, T., Gasteiger, J., Kollman, P. A., Eds.; Wiley: Chichester, U.K., 1998; Vol. 3, pp 1792−1811. (b) Weinhold, F.; Landis, C. R. *Chem. Educ.: Res. Pract. Eur.* **2001**, *2*, 91–104.

(30) (a) Flapan, E. *When Topology Meets Chemistry: A Topological Look at Molecular Chirality*; Cambridge University Press: Cambridge, U. K., 2000, p 83. (b) Mark, A. G.; Forster, M.; Raval, R. *Tetrahedron: Asymmetry* **2010**, *21*, 1125–1134.

(31) Gillespie, R. J. *Coord. Chem. Rev.* **2008**, *252*, 1315–1327.

(32) Politzer, P.; Murray, J. S. *Chem. React. Theory* **2009**, 243–254.